Slow Binding of Metal Ions to Pigeon Liver Malic Enzyme: A General Case†

Hui-Chih Hung,*,‡ Gu-Gang Chang,‡ Zhiru Yang,§ and Liang Tong§

Department of Biochemistry, National Defense Medical Center, Taipei 114, Taiwan, and Department of Biological Sciences, Columbia University, New York, New York 10027

Received July 5, 2000; Revised Manuscript Received August 17, 2000

ABSTRACT: Pigeon liver malic enzyme was inhibited by lutetium ion through a slow-binding process, which resulted in a concave down tracing of the enzyme activity assay. The fast initial rates were independent of lutetium ion concentration, while the slow steady-state rates decreased with increasing Lu^{3+} concentration. The observed rate constant for the transition from initial rate to steady-state rate, k_{obs}, exhibited saturation kinetics as a function of Lu^{3+} concentration, suggesting the involvement of an isomerization process between two enzyme forms (R-form and T-form). The binding affinity of Lu^{3+} to the R-form is weaker ($K_{d,Lu} = 14\ \mu M$) than that of Mn^{2+} ($K_{m,Mn} = 1.89\ \mu M$); however, Lu^{3+} has much tighter binding affinity with the T-form ($K^*_{d,Lu} = 0.83\ \mu M$). Lu^{3+} was shown to be a competitive inhibitor with respect to Mn^{2+}, which suggests that Lu^{3+} and Mn^{2+} are competing for the same metal binding site of the enzyme. These observations are in accordance with the available crystal structure information, which shows a distorted active site region of the Lu^{3+}-containing enzyme. Other divalent cations, i.e., Fe^{2+}, Cu^{2+}, or Zn^{2+}, also act as time-dependent slow inhibitors for malic enzyme. The dynamic quenching constants of the intrinsic fluorescence for the metal-free and Lu^{3+}-containing enzymes are quite different, indicating the conformational differences between the two enzyme forms. The secondary structure of these two enzyme forms, on the other hand, was not changed. The above results indicated that replacement of the catalytically essential Mn^{2+} by other metal ions leads to a slow conformational change of the enzyme and consequently alters the geometry of the active site. The transformed enzyme conformation, however, is unfavorable for catalysis. Both the chemical nature of the metal ion and its correct coordination in the active site are essential for catalysis.

Cytosolic malic enzyme [(*S*)-malate:$NADP^+$ oxidoreductase (oxaloacetate-decarboxylating), EC 1.1.1.40] is a tetrameric enzyme catalyzing the divalent metal ion (Mn^{2+} or Mg^{2+}) dependent reversible oxidative decarboxylation of L-malate to yield CO_2 and pyruvate, with concomitant reduction of $NADP^+$ to NADPH (*1*−*10*, and references therein). In a previous study on the crystal structure of human mitochondrial malic enzyme, this enzyme has been suggested to belong to a new class of oxidative decarboxylases (*11*). Both an open form without substrate and metal ion (*11*) and closed form with bound substrate analogue and all cofactors (*12*) of the enzyme are available now, which opens a new avenue of research on the structure−function relationship of this enzyme. Pigeon liver malic enzyme has an overall 56% sequence identity and as high as 71% sequence homology with that of human malic enzyme. The proposal of Asp-258 as a direct metal ligand by the Fe^{2+}-catalyzed oxidation (*13*) and site-directed mutagenesis (*14*) is corroborated by the crystal structure of human malic enzyme (*11, 12*). Many other essential groups detected by chemical modification or site-directed mutagenesis are also supported by the structural information (*8*−*10*, *15*, and references therein). It is reasonable to suggest that all malic enzymes have similar overall structure topology.

More recently, we found that lanthanide ions competitively inhibited malic enzymes with respect to Mn^{2+} (*16*). The structural work reveals a new conformation of the enzyme in complex with metal ion. In the present study, we describe a novel metal ion-induced slow binding inhibition of malic enzyme. The slow binding phenomenon induced by metal ions seems to be a general case for malic enzyme.

EXPERIMENTAL PROCEDURES

Preparation of Recombinant Pigeon Liver Malic Enzyme. The plasmids containing pigeon liver malic enzyme gene were transformed into BL21 (DE3) bacteria. The transformants were incubated in LB medium and induced by 1 mM isopropyl β-D-thiogalactopyranoside (IPTG). The cells were then harvested by centrifugation at 5000*g* for 5 min. After sonication, the recombinant enzyme was purified by two successive chromatographic steps, Q-Sepharose and adenosine-2′,5′-bisphosphate-agarose (*17*). The purified enzyme was routinely examined for purity by sodium dodecyl sulfate−polyacrylamide gel electrophoresis (SDS−PAGE) (*18*).

Enzyme Assay. Malic enzyme activity was assayed in triethanolamine-HCl buffer (66.7 mM, pH 7.4) at 30 °C

† This work was supported by the National Science Council, ROC (Frontiers in Sciences Program, Grant NSC 89-2312-B016-001 to G.G.C.) and by the National Science Foundation (Grant MCB-99-74700 to L.T.).

* To whom correspondence should be addressed. E-mail: ibio33@ndmctsgh.edu.tw. Phone: +886-2-8792-3100, ext. 18832. Fax: +886-2-87921544 or +886-2-29339996.

‡ National Defense Medical Center.

§ Columbia University.

10.1021/bi001534f CCC: $19.00
Published on Web 10/26/2000

according to the published procedure (*19*). An enzyme unit was defined as the enzyme amount that catalyzes the production of 1 μmol of NADPH/min under the assay conditions using an absorption coefficient of 6220 M^{-1} for the NADPH. Protein concentration was determined by the protein-dye binding method of Bradford (*20*). An M_r of 260 000 for the tetrameric enzyme was used in the calculation of k_{cat} values.

Kinetic Analysis of the Time-Dependent Curvature Enzyme Activity Assay. In the metal ion-induced time-dependent inhibition experiments, the enzyme was added to the assay mixture containing Mn^{2+} and various concentrations of the inhibitory metal ions and the absorbance at 340 nm was monitored continuously for 10−15 min. The progress curves were analyzed according to eq 1 for a hysteretic enzyme (*21*−*23*):

$$[P] = v_s t - [(v_s - v_i)/k_{obs}][1 - \exp(-k_{obs})] \quad (1)$$

where P is the NADPH formed represented by the A_{340nm} increase, v_i and v_s are initial and steady-state velocities of the reaction in the presence of metal ions. k_{obs} is the apparent first-order rate constant for the transition from v_i to v_s, and t is time.

Fluorescence Quenching Experiments. The details of the enzyme conformation were analyzed with quenching studies. Quenching titrations with acrylamide were performed at 30 °C in a Perkin-Elmer LB50 luminescence spectrometer by sequential addition of aliquots of concentrated acrylamide solution (6 M) into the enzyme solution. The excitation wavelength was set at 290 nm, and the fluorescence emission spectra were scanned from 300 to 400 nm. The integrated area between 320 and 360 nm of the fluorescence spectra were used for data analysis.

The inner filter effects due to acrylamide absorption were corrected according to eq 2 (*24*):

$$F_{corr} = F_{obs} 10^{(A_{ex} + A_{em})/2} \quad (2)$$

where F_{corr} and F_{obs} are the corrected and observed fluorescence, respectively; A_{ex} and A_{em} are the acrylamide absorptions at the excitation and emission wavelengths, respectively.

The fluorescence quenching data in the presence of acrylamide were first analyzed by the Stern−Volmer equation (eq 3) (*25*):

$$F_o/F = 1 + K_Q[Q] \quad (3)$$

where F_o and F are the fluorescence intensities in the absence and presence of the quencher, respectively. K_Q is the dynamic quenching constant, and [Q] is the quencher concentration. The plot of F_o/F versus [Q] is linear for a homogeneous population of emitting fluorophors.

In contrast, heterogeneous fluorophors may lead to a curved Stern−Volmer plot. In this case, the data were treated by fitting to a modified Stern−Volmer equation (eq 4) (*26*):

$$F_0/(F_0 - F) = 1/([Q]f_a K_Q) + 1/f_a \quad (4)$$

where f_a is the fraction number of accessible fluorophors. The plot of $F_0/(F_0 - F)$ versus 1/[Q] gives a linear plot and allows a graphical determination of f_a and K_Q.

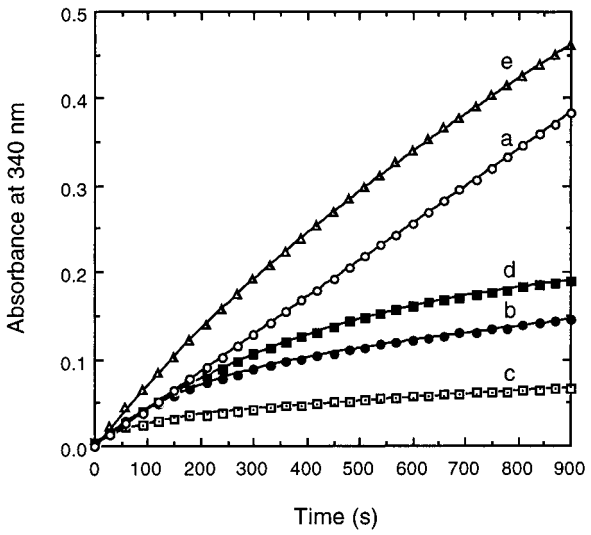

FIGURE 1: Progress curves of the pigeon liver malic enzyme in the absence or presence of metal ions in addition to Mn^{2+}. Trace a (○), standard enzyme assay with $MnCl_2$ in the reaction mixture. Traces b−e, same enzyme assay as trace a but with extra $LuCl_3$ (●, 30 μM), $FeCl_2$ (□, 0.2 mM), $CuCl_2$ (■, 50 μM), or $ZnCl_2$ (△, 0.8 mM), respectively, in the assay solution. The lines are computer fitted results according to eq 1. In each assay, total of 180 data points were used in fitting. Only 35 data points are shown for clarity.

Circular Dichroism Experiment. The possible metal ion-induced conformational change at the secondary structural level was examined by circular dichroism spectroscopy. The spectropolarimetric analysis was performed by monitoring the circular dichroism spectrum of the enzyme at 30 °C under constant N_2 flush in a Jasco J-810 spectropolarimeter from 200 to 250 nm. A quartz cuvette with a 1-mm light path was used. The enzyme with equal protein concentration with or without added metal ions was compared directly after a blank correction without added enzyme.

RESULTS

Time-Dependent Inhibition of Pigeon Liver Malic Enzyme by Lutetium Ion. Inhibition of malic enzyme by lutetium ion was a time-dependent process. During the assay period, the absorbance at 340 nm versus time exhibited a downward curve when lutetium ion was included in the assay mixture (Figure 1, trace b). There is a fast initial velocity (v_i), which slows down as the reaction progresses and finally reaches a constant steady-state velocity (v_s). It is the final steady-state rates that were used in analyzing the competitive inhibition behavior (*16*), which, however, lost a great deal of details of Lu^{3+} inhibition mechanism.

As shown in Figure 1, without lutetium ion, the A_{340nm} versus time plot was linear (Figure 1, trace a). The possible artifact of the curvature due to substrate depletion thus can be ruled out. The inhibition induced by Lu^{3+} represents a traditional slow binding process. The downward progress curves obtained from various concentrations of lutetium ion were fitted to eq 1 to estimate the v_i, v_s, and k_{obs}, i.e., the transition rate constant from v_i to v_s.

A slow binding inhibitor can affect the enzyme activity in several ways. The values of k_{obs}, obtained from fitting the kinetic data to eq 1, as a function of metal ion concentration were further used to differentiate the following mechanisms. eqs 5 and 6 are based on a slow binding

mechanism (mechanism A) as shown in reaction I (*21*−*23*, *27*−*29*).

mechanism A

$$E + M^{n+} \underset{k_4}{\overset{k_3}{\rightleftharpoons}} E{\cdot}M^{n+} \quad (I)$$

$$k_{obs} = k_4[1 + [M^{n+}]/K_{d,M(app)}] \quad (5)$$

$$K_{d,M(app)} = k_4/k_3 \quad (6)$$

where M^{n+} represents metal ion, while $n = 2$ or 3; k_3 and k_4 are association and dissociation rate constants of the $E{\cdot}M^{n+}$ binary complex, respectively. $K_{d,M(app)}$ is the apparent dissociation constant for the complex between enzyme and metal ion.

Equations 7 and 8 are derived from an enzyme isomerization mechanism (mechanism B, reaction II).

mechanism B

$$E + M^{n+} \underset{k_4}{\overset{k_3}{\rightleftharpoons}} E{\cdot}M^{n+} \underset{k_6}{\overset{k_5}{\rightleftharpoons}} E^*{\cdot}M^{n+} \quad (II)$$

$$k_{obs} = k_6 + \{k_5[M^{n+}]/(K_{d,M(app)} + [M^{n+}])\} \quad (7)$$

$$K^*_{d,M(app)} = K_{d,M(app)}\, k_6/(k_5 + k_6) \quad (8)$$

where E* represents an alternative enzyme conformation induced by the metal ion other than Mn^{2+} or Mg^{2+}, in this case the T-form; k_5 and k_6 are the forward and reverse isomerization rate constants, respectively. $K^*_{d,M(app)}$ is related to $K_{d,M(app)}$, k_5, and k_6 by eq 8. It could be considered as the apparent dissociation constant for the $E^*{\cdot}M^{n+}$ complex.

Kinetic data based on mechanism A is expected to show a linear dependence of k_{obs} on Lu^{3+} concentration, which is not consistent with the data shown in Figure 2. Figure 2 shows that the initial velocity (v_i) was independent of lutetium ion concentration, while the steady-state velocity (v_s) showed a hyperbolic dependence on Lu^{3+} concentration (Figure 2A). The transition rate constant, k_{obs}, showed a hyperbolic dependence on Lu^{3+} concentration and had a definite asymptote at the *y*-axis (Figure 2B). This result strongly suggests that the inhibition involved an isomerization process of the enzyme molecule in accordance with mechanism B. The curve was thus fitted to eq 7 to estimate the forward isomerization rate constant (k_5), the reverse isomerization rate constant (k_6), and the dissociation constant for the enzyme−lutetium ion complex [$K_{d,Lu(app)}$], which were found to be 0.71 ± 0.03 min^{-1}, 0.045 ± 0.013 min^{-1}, and 14 ± 1.9 μM, respectively (Table 1). The data were further fitted to eq 8 to estimate the second dissociation constant, $K^*_{d,Lu(app)}$, for the T-form of the enzyme. The value was calculated to be 0.83 ± 0.31 μM, which was consistent with the data obtained from steady-state inhibition experiment (0.91 ± 0.06 μM) (*16*). The value of $K^*_{d,Lu(app)}$, which is 17-fold smaller than $K_{d,Lu(app)}$ indicated that the T-form enzyme has a higher affinity for lutetium ion.

Other Divalent Ions Act as Time-Dependent Slow Inhibitors of Malic Enzyme. Pigeon liver malic enzyme is known to be very sensitive to the metal-catalyzed oxidative modification by Fe^{2+} or Cu^{2+} in the presence of ascorbate (*13*, *30*). To test this slow binding of metal ion to the enzyme,

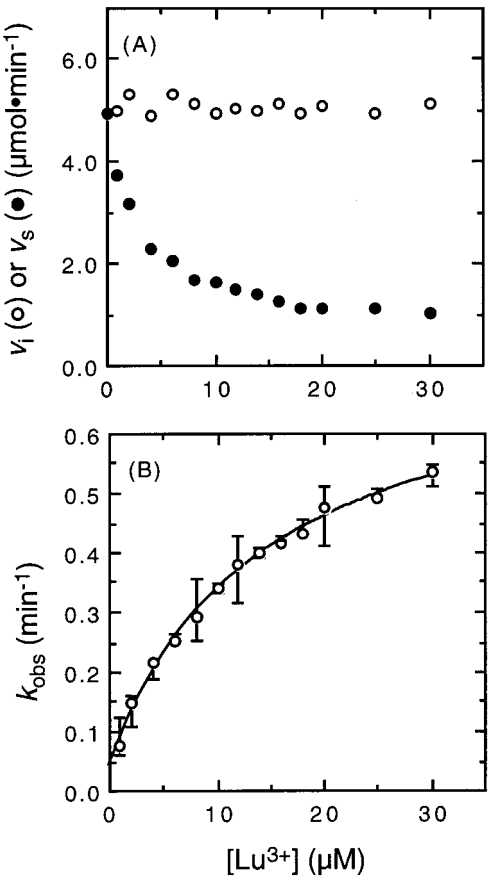

FIGURE 2: Slow binding inhibition of pigeon malic enzyme by lutetium ion. The progress curves similar to that shown in curve b of Figure 1 but with various concentrations of $LuCl_3$ were recorded for 15 min at 30 °C and the data were fitted to eq 1. (A) Initial velocity, v_i (○), or steady-state velocity, v_s (●), versus Lu^{3+} concentration plot. (B) The first-order rate constants (k_{obs}) for the transition from v_i to v_s process were plotted versus Lu^{3+} concentration. The hyperbolic curve was fitted to eq 7, which describes a slow enzyme isomerization process. The error bars in panel B indicate the fitting errors of the respective theoretical k_{obs} value.

the inhibition of malic enzyme by Zn^{2+}, Fe^{2+}, and Cu^{2+} was examined. All metal ions tested exhibited downward progressive traces (Figure 1). The downward progress curves at various metal ion concentrations were also fitted to eq 1 to estimate the v_i, v_s, and k_{obs} values. Both the observed values of v_i and v_s showed a descending hyperbolic tendency versus Fe^{2+} and Cu^{2+} concentrations (Figure 3, panels A and B). The slow inhibition induced by zinc ion was quite unique. Both v_i and v_s were activated by low Zn^{2+} concentrations but were inhibited at higher Zn^{2+} concentrations (Figure 3C). Saturation kinetics for the k_{obs} values as a function of metal ion concentration were shown in Figure 3 (panels D−F). Fitting the data to eq 7 and eq 8 allows the estimation of k_5, k_6, $K_{d,M(app)}$, and $K^*_{d,M(app)}$ for these metal ions (Table 1). For Fe^{2+}, the forward and reverse rate constants of the enzyme isomerization process were similar (0.087 ± 0.005 and 0.112 ± 0.005 min^{-1}, for k_5 and k_6, respectively), and the dissociation constant for Fe^{2+} from the R-form enzyme [$K_{d,Fe(app)} = 126 \pm 35$ μM] was about 2-fold larger than that from the T-form enzyme ($K^*_{d,Fe(app)} = 71 \pm 20$ μM). The differences between the forward and reverse rate constants k_5, and k_6, and between the dissociation constants $K_{d,Cu(app)}$ and $K^*_{d,Cu(app)}$ were above 30-fold for Cu^{2+} and above 60-

Table 1: Kinetic Parameters for the Time-Dependent Inhibition of Malic Enzyme by Metal Ions

kinetic parameters[a]	Lu^{3+}	Fe^{2+}	Cu^{2+}	Zn^{2+}
k_5 (min^{-1})	0.71 ± 0.03	0.087 ± 0.005	1.86 ± 0.25	0.51 ± 0.01
k_6 (min^{-1})	0.045 ± 0.013	0.112 ± 0.005	0.056 ± 0.018	0.008 ± 0.004
k_5/k_6 ratio	15.8	0.78	33.2	63.8
$K_{d(app)}$ (μM)	14 ± 1.9	126 ± 35	235 ± 57	480 ± 30
$K^*_{d(app)}$ (μM)	0.83 ± 0.31	71 ± 20	6.7 ± 2.3	7.4 ± 4.0

[a] These values were derived from Figure 2B and Figure 3, panels D−F, by fitting the results to eq 7 and eq 8.

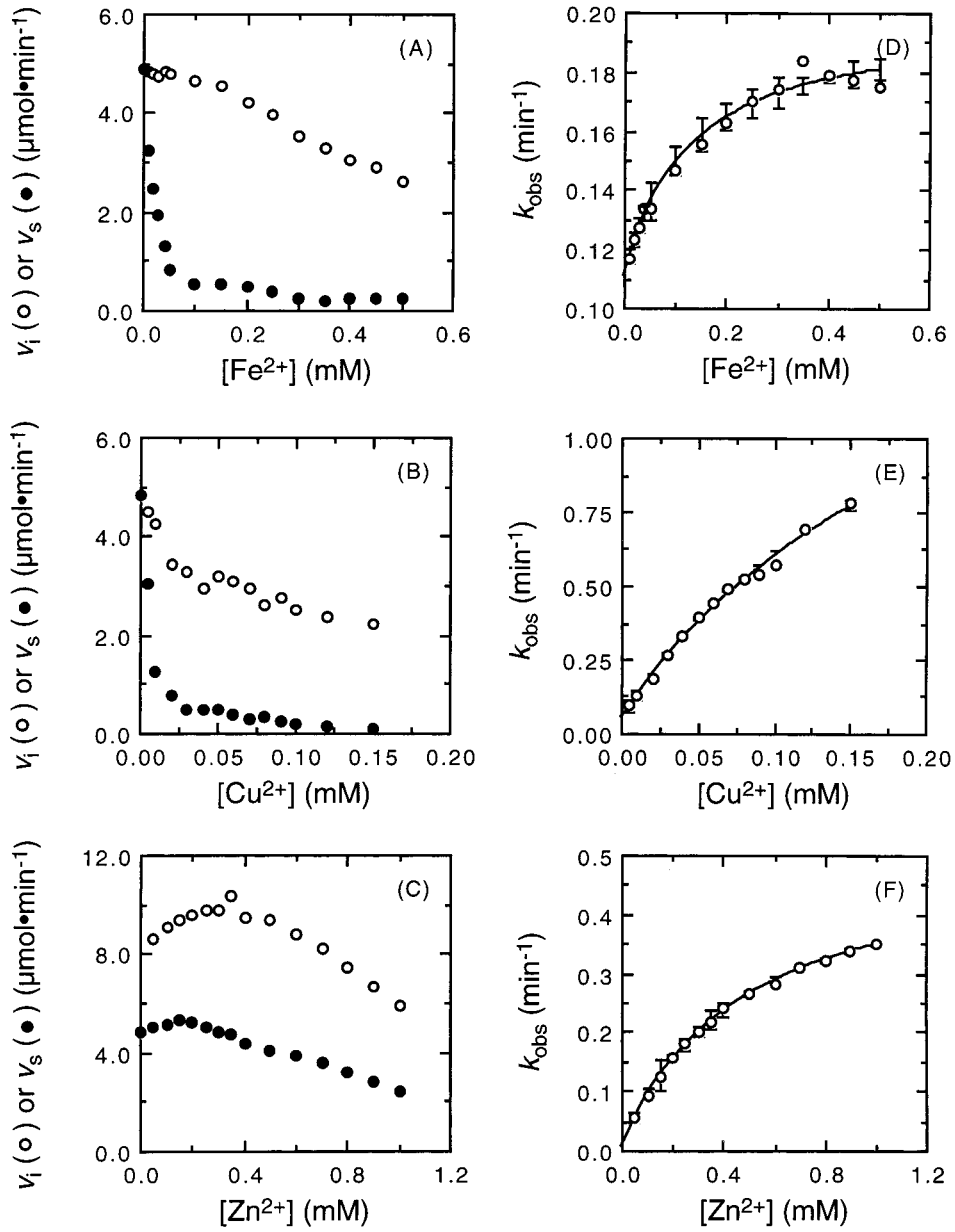

FIGURE 3: Slow binding inhibition of malic enzyme by other divalent ions. The progress curves were monitored at 30 °C for 15 min in the presence of various concentrations of $FeCl_2$, $CuCl_2$, or $ZnCl_2$. The progress curves were then fitted to eq 1. (A−C) Initial velocity, v_i (○), or steady-state velocity, v_s (●), versus [Fe^{2+}], [Cu^{2+}], or [Zn^{2+}], respectively. (D−F) The first-order rate constants (k_{obs}) for the transition from v_i to v_s process versus [Fe^{2+}], [Cu^{2+}], or [Zn^{2+}] plot, respectively. These hyperbolic curves were fitted to eq 7. The error bars in (D−F) represent the fitting errors of each theoretical k_{obs} value.

fold difference for Zn^{2+}. This means that the equilibrium switches from R-form to T-form in the presence of copper or zinc ion.

Reactivation of the Lutetium-Inhibited Pigeon Liver Malic Enzyme by Manganese Ion. There are two lines of evidence indicating that the metal-induced enzyme isomerization is a reversible process. First, the fitted data shown in Figures 2B and 3, panels D−F, did not result in curves going through the origin, which indicates a nonzero reverse rate (k_6). Second, the Lu^{3+}-inhibited enzyme activity could be restored by high concentration of manganese ion, which drives the conversion of T-form malic enzyme back to the catalytically active R-form (Figure 4). The Lu^{3+}-inhibited enzyme activity was gradually recovered. These experimental results also

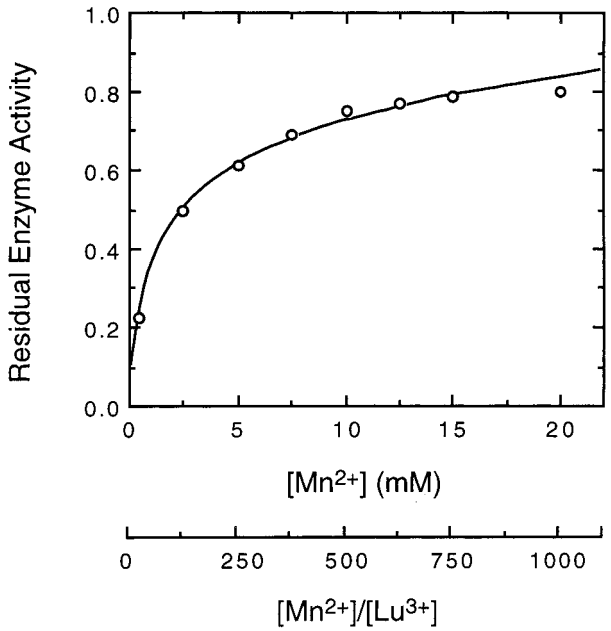

FIGURE 4: Regeneration of the lutetium-inhibited malic enzyme activity by manganese ion. The enzyme was preincubated with 20 μM $LuCl_3$ at 30 °C for 30 min. Various amounts of Mn^{2+} was then added into the solution and the system was allowed to equilibrate for 1 h and then steady-state enzyme activity was assayed. In assay mixture, Lu^{3+} concentration was kept constant at 20 μM.

exclude protein instability as the possible reason for the curvature enzyme assay trace shown in Figure 1. The time-dependent process represents the enzyme isomerization from the T-form back to the R-form. The inhibited enzyme activities by other divalent metal ions also could be recovered by manganese ion, and all showed a slow process (data not shown). The slow binding of metal ion to malic enzyme seems to be a general phenomenon.

Structural Comparison of Malic Enzyme with Different Metal Ions. Circular dichroism spectra of the metal-free and Mn^{2+}- or Lu^{3+}-containing malic enzyme are almost identical (data not shown). The secondary structure of the enzyme does not seem to be altered by the binding of manganese or lutetium ion with malic enzyme, which corroborates with the crystal structure information (*16*). Acrylamide quenching experiments were performed to examine the possible effect of metal ions on the tertiary structure of the enzyme (Figure 5). There was no obvious tertiary structural change in the enzyme when Mn^{2+} was included. The dynamic quenching constant (K_Q) values were 4.51 ± 0.64 and 4.78 ± 0.46 M^{-1}, respectively, for the metal-free and Mn^{2+}-containing enzyme ($[Mn^{2+}] = 10-50$ μM) (Table 2), which indicate that the R $\leftrightarrow$ T equilibrium favors to the left (R-form). In contrast, a significant tertiary structural change of the enzyme induced by lutetium ion was observed. Incubation of the metal-free enzyme with lutetium ion results in a significant increase in dynamic quenching constant (K_Q range from 6.55 ± 0.28 to 13.05 ± 0.84 M^{-1} at $[Lu^{3+}] = 10-50$ μM) suggesting a conformational change accompanied by lutetium ion occupation at the metal binding site of the enzyme. The nonlinear Stern−Volmer plot for the Lu^{3+}-enzyme, however, indicates heterogeneous microenvironments of the tryptophanyl residues in the enzyme molecule. The change of fractional accessible fluorophors (f_a) further indicates conformational changes induced by Lu^{3+} (Table 2).

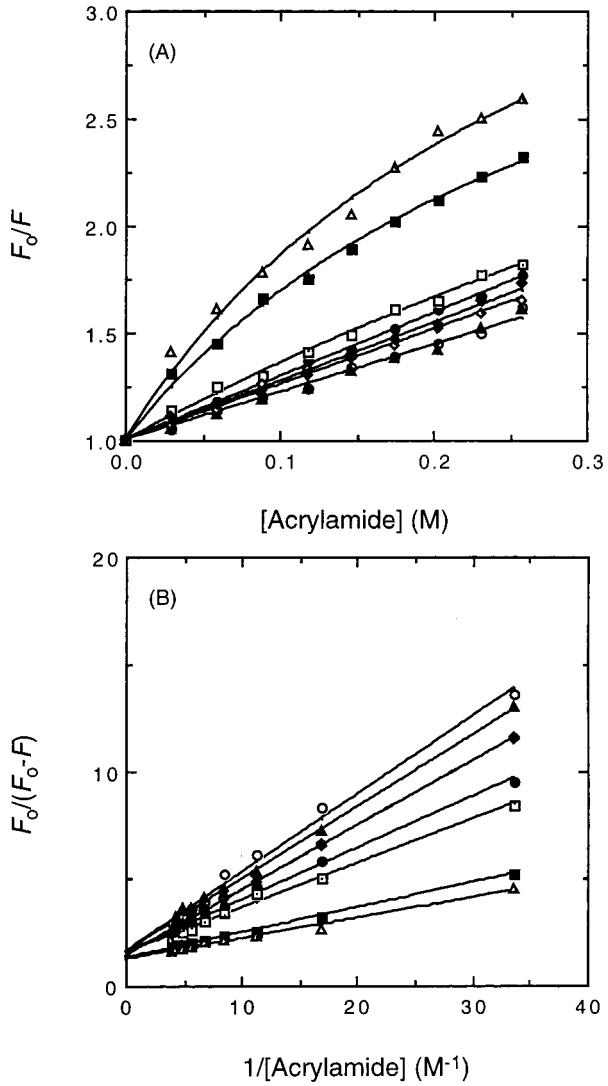

FIGURE 5: Quenching of intrinsic fluorescence of pigeon malic enzyme by acrylamide. The enzyme in Tris-acetate buffer (0.1 M, pH 7.5) was mixed with increasing amounts of acrylamide. The fluorescence spectra were then scanned upon excitation at 290 nm. The dilution and inner filter effects were corrected. (A) Stern−Volmer plot. (B) Lehrer plot. (○) Metal-free enzyme; the other symbols represent the enzyme preincubated with (●) 10 μM Lu^{3+}, (□) 20 μM Lu^{3+}, (■) 40 μM Lu^{3+}, (△) 50 μM Lu^{3+}, (▲) 10 μM Mn^{2+}, (◇) 40 μM Mn^{2+}, or (◆) 50 μM Mn^{2+}. The symbols are the experimental data and the lines are the computer fitted results according to a modified Stern−Volmer equation (eq 4).

Table 2: Fluorescence Quenching Parameters of Metal-Free and Metal-Containing Malic Enzyme[a]

metal ion	concentration (μM)	K_Q (M^{-1})	f_a
no metal	0	4.51 ± 0.64	0.61 ± 0.07
$[Mn^{2+}]$	10	4.84 ± 0.4	0.61 ± 0.04
	40	4.75 ± 0.13	0.70 ± 0.02
	50	4.78 ± 0.46	0.69 ± 0.05
$[Lu^{3+}]$	10	6.55 ± 0.61	0.63 ± 0.04
	20	7.57 ± 0.74	0.64 ± 0.04
	40	11.13 ± 0.35	0.77 ± 0.01
	50	13.05 ± 0.84	0.81 ± 0.03

[a] The data were derived from Figure 5 and calculated according to eq 4.

Figure 6 shows the superimposition of the crystal structures of the metal-free and the lutetium-containing malic enzyme.

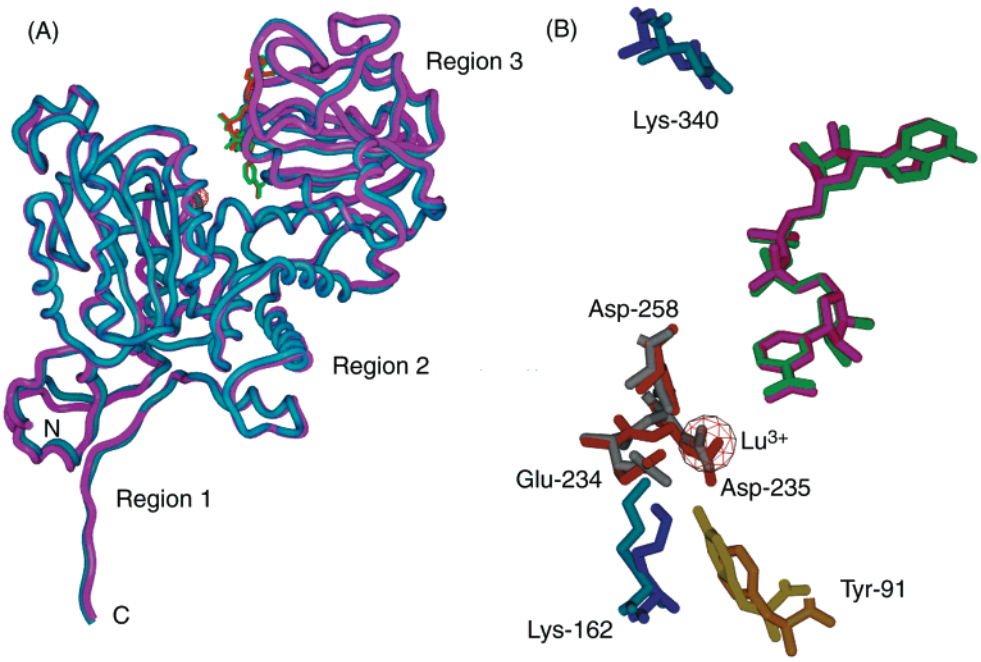

FIGURE 6: Superimposition of the crystal structures of metal-free and Lu^{3+}-containing malic enzymes. (A) Comparison of the superimposed open form malic enzyme (PDB code 1qr6) (*11*) and lutetium-containing malic enzyme from human mitochondria (*16*). The rms deviation between these two structures is 1.059 Å. The enzyme without metal ion is shown by sky-blue worm. The lutetium-containing enzyme is shown by purple worm, where the lutetium atom is shown as red sphere. The bound nucleotide is shown in green for the metal-free enzyme or red for the lutetium-containing enzyme. (B) Superimposition of the essential amino acid residues at the active site region. Residues from the metal-free enzyme are shown in yellow (Tyr-91), cyan (Lys-162, Lys-340), and gray (Glu-234, Asp-235 and Asp-258); and those for lutetium-containing enzyme are shown in orange (Tyr-91), dark blue (Lys-162, Lys-340), red (Glu-234, Asp-235, and Asp-258). The nucleotide are shown in green and violet, respectively, for the metal-free and Lu^{3+}-containing enzyme. The amino acid residue numbering system is for pigeon enzyme. For human enzyme, 21 should be added to the corresponding numbers. This figure is generated with the SPOCK program [web site: http://quorum.tamu.edu/jon/spock/ (accessed 8/10/1998)].

In accordance with the CD spectra, the secondary structure of lutetium-containing enzyme is almost identical to the metal-free enzyme. However, the overall tertiary topology between the metal-free and lutetium-containing enzyme is different. Similar to the open form to closed form transition of the enzyme (*12*), the conformational differences between metal-free and Lu^{3+}-containing enzymes are mostly due to relative movements among three regions of the molecule (Figure 6A). Region 2 of metal-free enzyme is above, but regions 1 and 3 are behind the Lu^{3+}-containing enzyme. In the active site region, the tertiary structure of the Lu^{3+}-enzyme has been somewhat distorted (Figure 6B). These structural data are consistent with the quenching experimental results, which indicate a profound effect of lutetium ion on the enzyme conformation. Several essential amino acid residues have their distance and orientation altered in Lu^{3+}-containing enzyme. The carboxylic groups of Glu-234, Asp-235, and Asp-258 are more closely in lutetium-containing enzyme. The geometric alteration of the catalytically essential groups Tyr-91 and Lys-162 (*12*, *15*) or the 2′-phosphate binding ligand of $NADP^+$, Lys-340 (*15*), might correspond to the inhibition of enzyme activity.

DISCUSSION

A number of enzymatic reactions do not respond instantaneously to the presence of a competitive inhibitor, but rather show a slow onset of the inhibition (*21*). Two mechanisms have been proposed for such slow binding inhibition (*22*, *23*). Mechanism A assumes that formation of an EI complex is the slow step because the concentration of inhibitor is small or the inhibitors encounter barriers to its binding site of the enzyme. Mechanism B, which is more general, assumes a rapid formation of EI complex but undergoes a slow enzyme isomerization process.

Pigeon liver malic enzyme requires a metal ion, e.g., manganese or magnesium ion, for catalysis. Substitution of manganese or magnesium ion at the metal binding site by lutetium ions strongly inhibits the enzyme activity. The inhibition involves an enzyme conformational change. The molecular basis of these kinetic observations was elucidated from the structural information.

The divalent metal ion Mn^{2+} or Mg^{2+} is octahedrally coordinated by the enzyme and is essential for the enzymatic activity. The coordination involves Asp-258, Glu-234, Asp-235, and two carboxylate groups from the substrate plus a water molecule in the active center (*12*). We show that replacement of the essential metal ion by some other metal ions (Lu^{3+}, Fe^{2+}, Cu^{2+}, Zn^{2+}) inhibits the enzyme activity, presumably due to a metal ion-induced slow transformation of the enzyme molecule from the enzymatically active relaxed form to an inactive or less active tight form. The binding of a transition metal ion to an enzyme with high affinity and high specificity requires discrimination in size, charge, and chemical nature of the metal ion (*31*, *32*). Mn^{2+} is characterized as "hard" and predominantly tends to coordinate with the carboxylate oxygens of asparate or glutamate (*33*). In malic enzyme, Mn^{2+} is bound with six liganding oxygen atoms arranged in an octahedral coordination (*12*, *33*, *34*). In contrast, Zn^{2+}, Cu^{2+}, and Fe^{2+}, which are characterized as metal ions of "borderline hardness", have

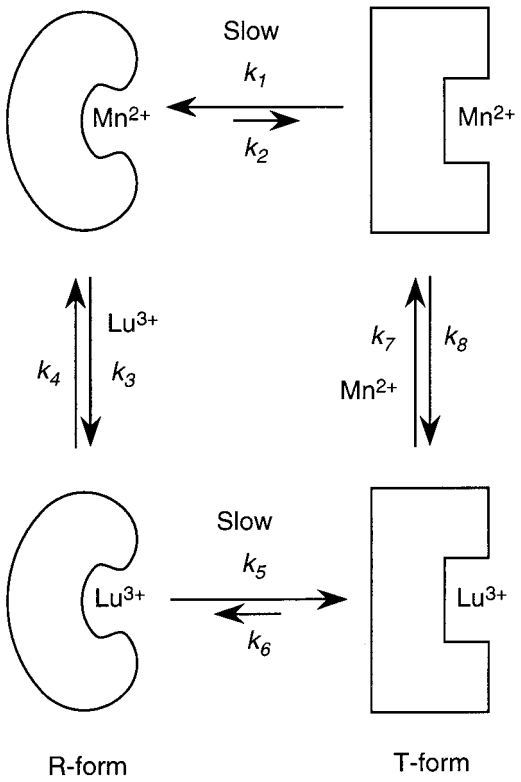

FIGURE 7: Schematic model for the metal-dependent interconversion of two forms of malic enzyme. The active form is referred as the relaxed form (R-form). Binding of Lu^{3+} at the Mn^{2+} binding site transforms the enzyme into a less active or inactive tight form (T-form). In presence of Mn^{2+}, the enzyme favors to the catalytic competent R-form.

relatively small ionic radius and tend to complex with more diverse arrays of ligands in enzymes. In zinc metalloenzyme, metal coordination geometry is usually tetrahedral or distorted tetrahedral (coordination number = 4). The copper ion in malic enzyme might have a coordination number of 4 (*35*). An optimal enzyme-metal binding site will be complementary in chemical nature and prefers coordination geometry to the target of the metal ion for catalysis.

In lutetium ion inhibition, the value of $K_{d,Lu}$ (14 μM) is larger than $K_{m,Mn}$ (1.89 μM) but the $K^*_{d,Lu}$ (0.83 μM) is smaller than $K_{m,Mn}$. Moreover, the value of v_i is independent of metal ion concentration. Although the trivalent charge of lutetium ion supposed to be more attractive to the metal binding site, yet the bigger size of lutetium ion (atomic weight = 175) than manganese and other divalent ions (atomic weight 55−65) and their eight or nine coordination (*36*, *37*) may cause steric interference. Indeed, the initial interaction of enzyme and inhibitor may not necessarily be fast so that the Lu^{3+}-enzyme and Mn^{2+}-enzyme are in steady-state equilibrium (k_3, k_4 in Figure 7). The strong inhibition of malic enzyme by Lu^{3+} is manifested by its smaller $K_{d,Lu}$ and $K^*_{d,Lu}$, values as compared to other metal ions (Table 1). Charge effect might play a major role. Other lanthanide ions (La^{3+}, Pr^{3+}, Gd^{3+}, and Yb^{3+}) also exhibit various levels of inhibition to the human mitochondrial malic enzyme (*16*).

In accordance with the above results, we suggest that the slow binding phenomenon observed for lutetium inhibition on malic enzyme is due to a slow isomerization step between the R-form and T-form of the enzyme as illustrated in Figure 7. The T-form enzyme, which has higher affinity for lutetium ion, does not favor catalysis. This T-form malic enzyme may not be equivalent to the catalysis-competent intermediate form because the Mn^{2+}-enzyme and Lu^{3+}-enzyme have quite different tertiary structures (Figure 5). More likely, the enzyme is being trapped into a catalytically inactive or less active tight form as depicted in Figure 7.

In the case of Fe^{2+} and Cu^{2+}, since no ascorbate or other reductant was included in the reaction mixture and a saturating amount of Mn^{2+} was used in the routine assay, the enzyme was sufficiently protected from free-radical mediated oxidation (*13*, *30*). The decreased enzyme activity thus cannot be the result of metal-catalyzed oxidative modification. Displacement of Mn^{2+} by Cu^{2+} or Fe^{2+} at the metal binding site should be the reason for inhibition. Competitive inhibition of pigeon liver malic enzyme by Cu^{2+} with respect to Mn^{2+} had been demonstrated previously (*30*). In iron and copper ion inhibition, the initial velocity is descending with increasing metal ion concentrations. Because Cu^{2+} and Fe^{2+} have similar size and charge as compared to manganese ion, they bind rapidly to the enzyme, inhibit the enzyme activity instantaneously, the subsequent slow conformational change of the enzyme elicits further decrease in the enzyme activity. The different affinity cleavage patterns after oxidative modification of the enzyme by Fe^{2+} or Cu^{2+} (*30*) can be partially explained by the results shown in Table 1. The Fe^{2+}-enzyme favors the R-form, while the Cu^{2+}-enzyme favors the T-form as revealed by the k_5/k_6 ratios. While Fe^{2+}-ascorbate system correctly identified Asp-258 as the metal ligand (*11*−*14*); Cu^{2+}-ascorbate system under acidic condition cleaves the enzyme at some curious positions Asp-194 and Asp-464 (*30*, *38*), which are remote from the active site. It is possible that Cu^{2+} could bind to some multiple remote sites in addition to the active site.

Zn^{2+} and some other divalent metal ions can support the reaction, albeit at slow rate (*35*, *39*). The inhibition by zinc ion is unique, which occurred only at high zinc concentration. Both the initial and steady-state velocities increase at low Zn^{2+} concentrations. At high concentrations, Zn^{2+} induces a drop of both v_i and v_s (Figure 3C), probably due to the nonspecific binding of Zn^{2+} at some remote sites. Alternatively, Zn^{2+} has the largest k_5/k_6 ratio, which indicates very small R-form at R ⇔ T equilibrium. Assuming that the R ⇔ T transition step is intrinsically fast, then it is conceivable that a very slow binding process will be observed. Since $v = k[R]$, if [R] at equilibrium is very small, then v will be correspondingly slow even if k itself is very fast.

In summary, we propose, for the first time, a slow binding concept for the metal binding of malic enzyme. We propose that binding of metal ion to malic enzyme shifts equilibrium of the enzyme between two structural forms. The structural change induced by metal ion might be a general phenomenon for the enzyme going from opened nucleotide−enzyme binary complex to closed nucleotide−metal ion−substrate−enzyme quaternary complex.

REFERENCES

1. Frenkel, R. (1975) *Curr. Top. Cell. Regul. 9*, 157−181.
2. Goodridge, A. G., Klautky, S. A., Fantozzi, D. A., Baillie, R. A., Hodnett, D. W., Chen, W., Thurmond, D. C., Xu, G., and Roncero, C. (1996) *Prog. Nucleic Acid Res. Mol. Biol. 52*, 89−122.
3. Hsu, R. Y. (1982) *Mol. Cellu. Biochem. 43*, 3−26.

4. Hermes, J. D., Roeske, C. A., O'Leary, M. H., and Cleland, W. W. (1982) *Biochemistry 21*, 5106−5114.
5. Urbauer, J. L., Bradshaw, D. E., and Cleland, W. W. (1998) *Biochemistry 37*, 18026−18031.
6. Karsten, W. E., Hwang, C. C., and Cook, P. F. (1999) *Biochemistry 38*, 4398−4402.
7. Karsten, W. E., Chooback, L., Liu, D., Hwang, C. C., Lynch, C., and Cook, P. F. (1999) *Biochemistry 38*, 10527−10532.
8. Chou, W. Y., Liu, M. Y., Huang, S. M., and Chang, G. G. (1996) *Biochemistry 35*, 9873−9879.
9. Chou, W. Y., Huang, S. M., and Chang, G. G. (1997) *Protein Eng. 10*, 1205−1211.
10. Huang, S. M., Chou, W. Y., Lin, S. I., and Chang, G. G. (1998) *Proteins 31*, 61−73.
11. Xu, Y., Bhargava, G., Wu, H., Loeber, G., and Tong, L. (1999) *Structure 7*, 877−889.
12. Yang, Z., Floyd, D. L., Loeber, G., and Tong, L. (2000) *Nat. Struct. Biol. 7*, 251−257.
13. Wei, C. H., Chou, W. Y., Huang, S. M., Lin, C. C., and Chang, G. G. (1994) *Biochemistry 33*, 7931−7936.
14. Wei, C. H., Chou, W. Y., and Chang, G. G. (1995) *Biochemistry 34*, 7949−7954.
15. Kuo, C. C., Tsai, L. C., Chin, T. Y., Chang, G. G., and Chou, W. Y. (2000) *Biochem. Biophys. Res. Commun. 270*, 821−825.
16. Yang, Z., Batra, R., Floyd, D. L., Hung, H. C., Chang, G. G., and Tong, L. (2000) *Biochem. Biophys. Res. Commun*. *274*, 440−444.
17. Chang, G. G., Wang, J. K., Huang, T. M., Lee, H. J., Chou, W. Y., and Meng, C. L. (1991) *Eur. J. Biochem. 202*, 681−688.
18. Chang, G. G., Huang, T. M., Huang, S. M., and Chou, W. Y. (1994) *Eur. J. Biochem. 225*, 1021−1027.
19. Chang, G. G., Huang, T. M., Wang, J. K., Lee, H. J., Chou, W. Y., and Meng, C. L. (1992) *Arch. Biochem. Biophys. 296*, 468−473.
20. Bradford, M. M. (1976) *Anal. Biochem. 72*, 248−254.
21. Frieden, C. (1979) *Annu. Rev. Biochem. 48*, 471−489.
22. Neet, K. E., and Ainslie, G. R., Jr. (1980) *Methods Enzymol. 64B*, 192−226.
23. Copeland, R. A. (1996) *Enzymes*, pp 237−261, Wiley-VCH, New York.
24. Lakowicz, J. R. (1983) *Principles of Fluorescence Spectroscopy*, p 44, Plenum, New York.
25. Eftink, M. R., and Ghiron, C. A. (1981) *Anal. Biochem. 114*, 199−227.
26. Lehrer, S. S. (1971) *Biochemistry 10*, 3254−3262.
27. Morrison, J. F. (1982) *Trends Biochem. Sci. 7*, 102−105.
28. Morrison, J. F., and Walsh, C. T. (1988) *Adv. Enzymol. 61*, 201−301.
29. Sculley, M. J., Morrison, J. F., and Cleland, W. W. (1996) *Biochim. Biophys. Acta 1298*, 78−86.
30. Chou, W. Y., Tsai, W. P., Lin, C. C., and Chang, G. G. (1995) *J. Biol. Chem. 270*, 25935−25941.
31. Christianson, D. W. (1997) *Prog. Biophys. Mol. 67*, 217−252.
32. Christianson, D. W., and Cox, J. D. (1999) *Annu. Rev. Biochem. 68*, 33−57.
33. Pearson, R. G. (1963) *J. Am. Chem. Soc. 85*, 3533−3539.
34. Hsu, R. Y., Mildvan, A. S., Chang, G. G., and Fung, C. (1976) *J. Biol. Chem. 251*, 6574−6583.
35. Rutter, W. J., and Lardy, H. A. (1958) *J. Biol. Chem. 233*, 374−382.
36. Cotton, S. (1991) *Lanthanides and Actinides*, Oxford University Press, New York.
37. Cotton, F. A., and Wilkinson, G. (1988) *Advanced Inorganic Chemistry*, 5th ed., John-Wiley & Sons, New York.
38. Chou, W. Y., Chang, H. P., Huang, C. H., Kuo, C. C., Tong, L., and Chang, G. G. (2000) *Protein Sci. 9*, 242−251.
39. Grissom, C. B., and Cleland, W. W. (1988) *Biochemistry 27*, 2927−2934.

BI001534F